Precise Dynamic Turning of a 10 cm Legged Robot on a Low Friction Surface Using a Tail

N.J. Kohut† A.O. Pullin† D. W. Haldane† D. Zarrouk* and R. S. Fearing*

***Abstract*— For maximum maneuverability, terrestrial robots need to be able to turn precisely, quickly, and with a small radius. Previous efforts at turning in legged robots primarily have used leg force or velocity modulation. We developed a palm-sized legged robot, called TAYLRoACH. The tailed robot was able to make rapid, precise turns using only the actuation of a tail appendage. By rapidly rotating the tail as the robot runs forward, the robot was able to make sudden 90° turns at 360 $^\circ s^{-1}$. Unlike other robots, this is done with almost no change in its running speed. We have also modeled the dynamics of this maneuver, to examine how features, such as tail length and mass, affect the robot's turning ability. This approach has produced turns with a radius of 0.4 body lengths at 3.2 body lengths per second running speed. Using gyro feedback and bang-bang control, we achieve an accuracy of ± 5° for a 60° turn.**

I. Introduction

Small legged robots are a strong potential platform for a variety of tasks, from search and rescue operations in hazardous areas, to safety inspections in remote or inaccessible locations. Precise, rapid maneuverability can be the key to completing a task quickly and efficiently, and being able to complete small radius turns means the robot has access to smaller spaces. Terrestrial robots have found diverse solutions for locomotion, including jumping [1][16], inchworm like movement[13][17], a hybrid approach of walking and flying [22], and others. This paper presents TAYLRoACH (Tail Actuated Yaw Locomotion Robotic Autonomous Crawling Hexapod), a legged robot that can steer using differential drive from its legs or using its tail as an inertial appendage to produce a precise turn in a small space. Previous work has shown that turning with a tail can produce rapid turns [24] [14]. This paper demonstrates the ability to do this precisely, and supplies a more comprehensive analysis of executing terrestrial turns with a tail. Below, we review previous work in legged steering and robotic tails.

The methods legged robots use to turn vary greatly. In previous work, we showed that legged robots can turn using differential velocity drive, varying the speeds of their legs to induce a turn through kinematics [24]. It was also shown that a tail with open loop actuation can induce rapid turns [24] [14]. RHex also uses a kinematic approach to turning, altering the amount of time each leg is on the ground while keeping the overall leg frequencies constant [21]. Differential leg stiffness has also been shown to induce turning [7]. Rapid turning has been shown by actively changing leg kinematics in Sprawlita [3] and iSprawl [20]. MiniRoACH [6] uses differences in left/right gait timing to turn, while MEDIC [15], a small, SMA-actuated robot, turns by driving one set of legs forwards while driving another set of legs backwards. DASH [2] is a compliant robot that turns by warping its body, thus altering its gait.

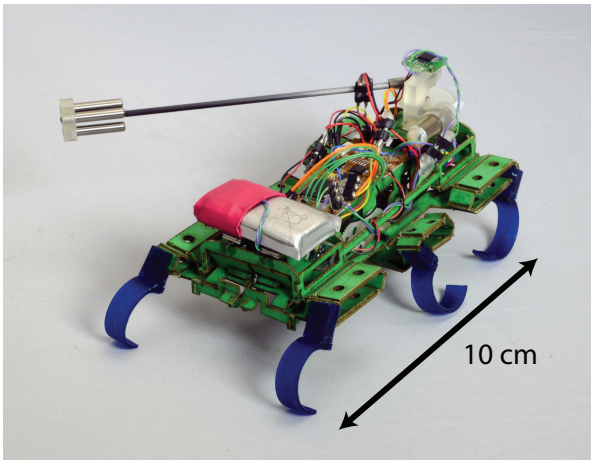

Fig. 1. TAYLRoACH, a 48 gram legged robot, able to run at over 1 m/s and turn at over 400 $^\circ s^{-1}$.

Animals use tails for many purposes, from communication and mating, to balance and attitude control while airborne [10]. Robots have also applied tails for a variety of purposes. Climbing robots often use a tail to provide normal force against the climbing surface, producing an anti-peeling moment [26][23][11][19]. Aquatic robots have used tails for turning based on hydrodynamic forces [5]. Tails have also been used on robots to control pitch and orientation [27] while airborne, ensuring the robot lands on its feet [9][4][18]. Here we explore the use of the tail for yaw turning using angular momentum exchange, but also with complex ground interaction and friction, not previously examined. Ground interaction introduces changing coefficients of friction, changes in normal forces, and other disturbances from leg motion not found when the robot is airborne.

II. Robot Design

A. TAYLRoACH

The TAYLRoACH is a hexapedal millirobot designed and fabricated using the Smart Composite Microstructures

This material is based upon work supported by the National Science Foundation under IGERT Grant No. DGE-0903711 and by the Army Research Laboratory under the Micro Autonomous Systems and Technology Collaborative Technology Alliance .

Corresponding author: kohut@berkeley.edu, † Dept. of Mechanical Engineering, University of California, Berkeley

* Dept. of Electrical Engineering and Computer Science, University of California, Berkeley

process [8]. Its six legs are driven by a brushed DC motor-powered rotary crank coupled to kinematic transmission linkages which translate the rotary input into useful leg motion. The geometry of these linkages was preserved from the DynaRoACH platform [7]; however they were optimized for dynamic performance and minimal hysteresis. The kinematics of these linkages effectively prescribe a leg gait with a duty factor of 0.5 and symmetric touchdown and liftoff angles of $\pm 42°$. Additionally, TAYLRoACH utilizes a split transmission to allow for robust steering control, effectively skid steering between the two disjoint sets of legs [24].

B. Tail Transmission Design

TAYLRoACH employs a 10.2 cm long tail that has a 4 gram weight on its end (see Section III-D). A previous design of a tail for this robot [14] used a spur gear transmission to drive the tail with a ratio of 85:1. A worm gear transmission is now employed, with the worm drive gear powering a single output gear. The transmission has a gear ratio of 60:1, allowing for high torque inputs to the tail so that the feet can overcome static friction forces when the tail is actuated. A 7mm coreless brushed DC motor provides power for the tail. The motor control electronics are described in section II-C. The output gear and transmission housing are custom 3D printed parts [1], allowing each to be a single rigid piece for high stiffness and low weight. In addition, the transmission housing has an integrated shaft that houses a magnet used both for bearing support and sensor readings through a 14-bit AMS AS5048B-HTSP-500 Hall effect absolute position encoder. The tail spar is a 2 mm diameter carbon fiber rod of mass 0.46 grams, and the weight on the end consists of steel dowel pins press fit into a custom 3D printed piece.

Custom manufacture of the tail parts is necessary to keep the part count, complexity, weight, and size of the tail low. Using the worm gear offers major packaging advantages over a spur gear transmission, since the motor and output gear can be mounted on top of the robot instead of behind, minimizing the static change in weight distribution due to the tail ballast. The total tail system weight is 10.5 grams, including the 4 gram weight. The tail has a range of motion of 265 degrees before it encounters the transmission housing, which serves as a stop and prevents the tail from colliding with the robot. The packaging constraint of a limited range of motion tail makes the control presented in Section V-A a necessity.

C. Power, Communication, and Control Hardware

The robot is equipped with a control board similar to that used in [15]. A component block diagram is presented in Figure 3. A dsPIC33F microcontroller coordinates all the control loops, motion timing, and communication functions of the robot. The board also hosts a 3-axis MEMS chip gyroscope, and three motor drivers. Drive for the leg-actuating motors is identical to the method in [24], where each of the two legs motors are driven by a single MOFSET, providing

[1]http://printin3d.com/3d-printers

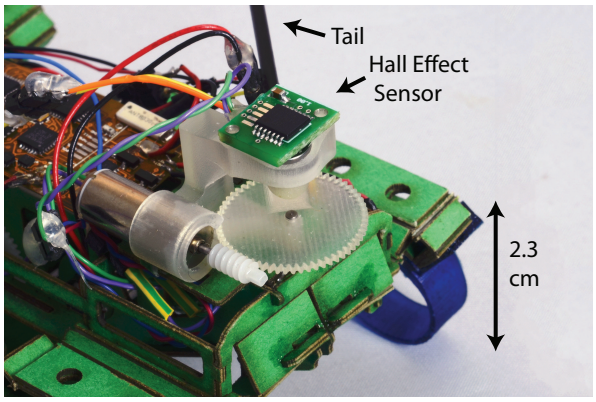

Fig. 2. The complete tail actuator, including motor, transmission, and absolute position sensor.

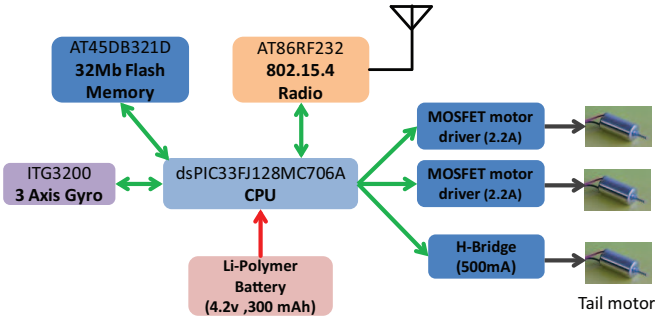

Fig. 3. Block diagram of controller board.

one-direction control with no braking. Leg motor speed is sensed via back-EMF, and average motor speed is controlled via pulse-width modulation (PWM) and a PID control loop. The drive for the tail motor is provided by an integrated chip H-bridge with a current limit of 0.5 A, resulting in limited motor torque, as discussed in Section III-B. The H-bridge is configured for no motor braking or current recirculation.

The magnetic position encoder for the tail described in Section II-B is connected to the CPU board via the I2C bus. Real-time telemetry is recorded onboard to a flash memory at 150 Hz and downloaded via an 802.15.4 radio after each experiment, providing a complete trace of the instantaneous inputs and outputs of each software control block, yaw rates, tail position, and motor back-EMF. After queues of motion commands are sent from a host PC system, the robot runs fully autonomously with no external control loop closure, all sensing done on-board, and millisecond accurate coordination of actuators and control goals.

III. Modeling

To model the turning of TAYLRoACH, we consider a point mass m_t on a massless rod of length l representing the tail, and a rigid body with mass m_b and yaw inertia I_b representing the robot body, as seen in Figure 4. The location where the tail is mounted to the body is referred to as the pin. Only planar dynamics are considered.

The robot has width $2a$ and length $2b$. The body's yaw angle relative to the world frame is θ. The tail's yaw angle

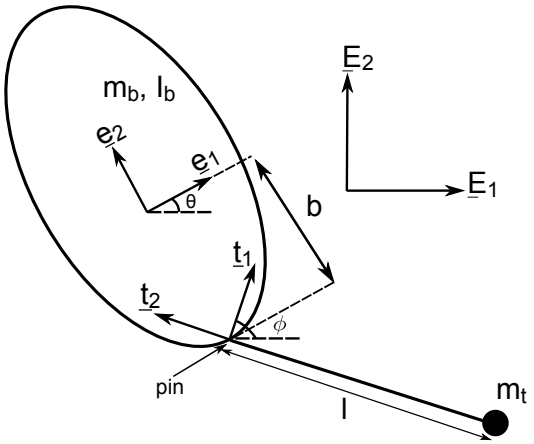

Fig. 4. Planar model of the robot body and tail.

relative to the world is ϕ. The relative angle of the tail and the body is ψ.

$$\psi = \theta - \phi \tag{1}$$

A. Balance of Moments

Analysis of tail-body dynamics while a robot is in free fall has been explored by [9][27]. The analysis presented below is similar but incorporates friction from the legs, a piecewise linear motor model, and compares turning with the tail to legged steering, also modeled here.

The angular momentum of the robot body can be expressed as

$$\mathbf{H_b} = \mathbf{I_b}\omega_\mathbf{b} + m_b\mathbf{r_b} \times \mathbf{v_b} \tag{2}$$

while the angular momentum of the tail can be expressed as

$$\mathbf{H_t} = m_t\mathbf{r_t} \times \mathbf{v_t} \tag{3}$$

where $\omega_\mathbf{b}$ is the angular velocity of the robot body, $\mathbf{r_b}$ and $\mathbf{r_t}$ are the body and tail position, and $\mathbf{v_b}$ and $\mathbf{v_t}$ are the body and tail velocity. All positions and velocities are relative to the combined body and tail system center of mass. We assume that prior to tail actuation the robot is running at steady state and that the net friction force is zero. The tail and body are both acted upon by an equal and opposite moment provided by the motor, and an equal and opposite reaction force at the pin. After actuation, we assume the body has a friction moment acting on it, but no net friction force (the friction is symmetric when the body turns). Since the pin force is the only net force on the body, it can be calculated as

$$\mathbf{F_{pin}} = m_b\mathbf{a_b} \tag{4}$$

From here, we can calculate equations of motion based on the change in angular momentum and the net moments on the tail and body.

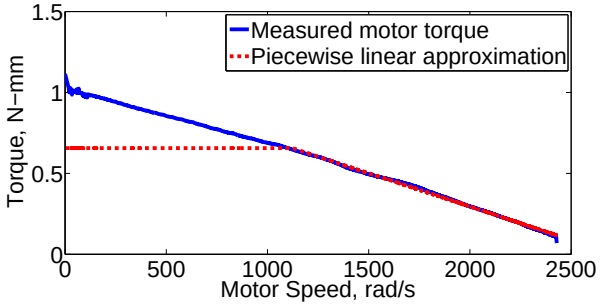

Fig. 5. Measured motor torque compared to the approximated motor torque used in the model.

$$\dot{\mathbf{H}}_\mathbf{b} = -\mathbf{T} + \mathbf{r_{pin}} \times \mathbf{F_{pin}} + \mathbf{M_f} \tag{5}$$

$$\dot{\mathbf{H}}_\mathbf{t} = \mathbf{T} - \mathbf{r_{pin}} \times \mathbf{F_{pin}} \tag{6}$$

where $\mathbf{T} = T\mathbf{E_3}$ is the torque from the tail transmission, and $\mathbf{M_f}$ is the sliding friction moment on the body. These equations can be expanded to

$$\begin{bmatrix} b^2k + I_b & blk\cos(\psi) \\ blk\cos(\psi) & l^2k \end{bmatrix} \begin{bmatrix} \ddot{\theta} \\ \ddot{\phi} \end{bmatrix} = \begin{bmatrix} -T + M_f + blk\sin(\psi)\dot{\phi}^2 \\ T + blk\sin(\psi)\dot{\theta}^2 \end{bmatrix} \tag{7}$$

where

$$k = \frac{m_b m_t}{m_b + m_t} \tag{8}$$

This is calculated by the method presented in Section III-B. M_f is the moment on the robot body due to friction between the ground and the robot legs, discussed in Section III-C.

B. Motor Modeling

A Didel Superslicks 7mm brushed DC motor was used to drive the tail. Testing was performed on a dynamometer to determine motor torque as a function of motor speed. The H-bridge used to drive the motor can only provide 500 mA of current, limiting the motor's maximum torque. For this reason, a piecewise linear torque model was employed, as shown in Figure 5.

The motor speed and torque can be calculated as follows

$$\omega_{mot} = \eta\dot{\psi} \tag{9}$$

$$T_{mot} = \frac{T}{\eta\alpha} \tag{10}$$

where η is the gear ratio of the tail transmission and α is the mechanical efficiency of the drivetrain.

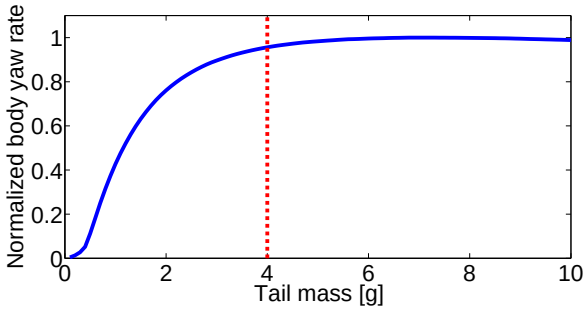

Fig. 6. Modeled normalized body yaw rate as a function of tail mass.

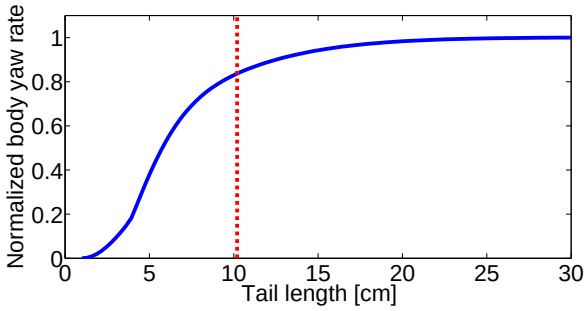

Fig. 7. Modeled normalized body yaw rate as a function of length.

C. Ground Interaction and Friction Moment

We use the Coulomb model to estimate the friction moment as the turn is made. We assume the friction produces a pure moment during the turn, and the friction moment is expressed as

$$M_f = -\mu_d(m_b + m_t)g \cdot r_{\text{eff}} \cdot \text{sgn}(\dot{\theta}) \tag{11}$$

where μ_d is the effective coefficient of friction, and r_{eff} is the effective radius of the moment. r_{eff} is defined to be half the diagonal length of the robot. The greatest tail torque occurs as soon as the tail is actuated, which overwhelms the static friction. As such, we only consider dynamic friction here. μ_d, which is a function of stride frequency, was measured experimentally by running the robot up a slope γ. If the robot was not able to advance upwards, but did not slide downwards, then the effective friction coefficient is

$$\mu_d = \arctan\gamma \tag{12}$$

This experiment was repeated for a range of leg frequencies between 0 and 13.3 Hz.

D. Model Sensitivity and Design

We can use the model to inform the design of the tail. By examining the sensitivity of the body yaw rate to tail length and mass we can choose a tail that will allow the robot to turn quickly and perform well in small spaces for maximum maneuverability.

Figure 6 presents the body yaw rate as a function of tail mass. The graph is normalized such that the maximum yaw rate over all masses has a value of 1. Diminishing returns can be found from increasing tail mass. Maximum yaw rate occurs with a 7 gram tail weight, but at 4 grams, we see 96% of the performance for less than 60% of the weight.

Figure 7 shows how the body yaw rate varies with tail length. The graph is normalized in the same way as Figure 6. Again, we see diminishing returns with an increasing tail length. Here, our length choice of 10.2 cm provides 84% of the maximum potential performance while keeping the tail length similar to the body length. Doubling the tail length to 20.4 cm would only give a 17% relative improvement over the 10.2 cm tail, but maneuverability would be greatly compromised.

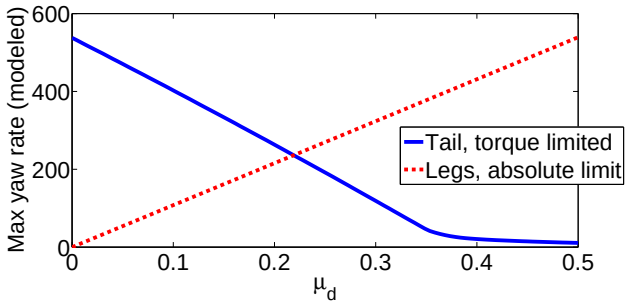

Fig. 8. As friction increases, legged turning becomes more effective, and tail turning loses effectiveness. However, the tail steering can be applied while the robot runs without losing forward speed. This would be difficult or impossible for the legged steering.

E. Comparing Theoretical Leg and Tail Yaw Rates

For turning with the tail, the motor torque limits the yaw rate. If more torque is available, the tail can be driven faster and the robot will turn faster. Legged turning however, is limited by friction and normal forces. We can determine a maximum theoretical turning limit for legs that are sliding on the ground and compare this to our tail turning method. For the best turning with the legs, we assume the legs on the outside of the turn are driving forward, while the legs on the inside of the turn are driving rearward. Eq. [13] shows the maximum moment that can be applied under sliding friction with the legs.

$$M_{\text{legs}} = \mu mg \cdot a \tag{13}$$

Applying this moment over time gives us the yaw rate of the body, which we can then compare to our model of tail turning as a function of dynamic coefficient of friction. The time used is 150 milliseconds, to accord with the physical experiments performed in section IV-B. Figure 8 shows the results of this comparison.

Without friction, the legs are unable to turn the robot at all, while the tail turns the robot at $530°s^{-1}$. At a friction coefficient of about 0.22, both methods are turning the robot at about $240°s^{-1}$. With a friction coefficient of 0.5, the tail can produce a yaw rate of only $10°s^{-1}$while the legs could theoretically produce $540°s^{-1}$. Legged turning in this manner would be difficult or nearly impossible while the robot is running at high speed, but this limitation does not apply to tail steering.

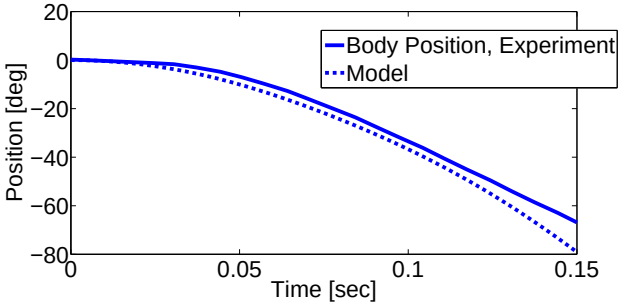

Fig. 9. The robot turns at almost $450°s^{-1}$in free fall. The model shows good agreement with the experiment.

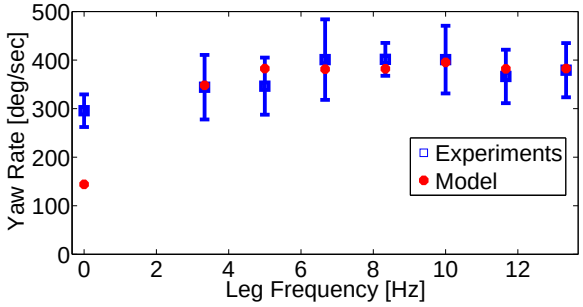

Fig. 10. Results from open loop trials on tile surface. The square markers indicate the mean yaw rate of the robot body during the experiments, while the bars show plus or minus one standard deviation away from this mean. The circles show results from the model detailed in section III. As leg frequency increases, turning performance increases and then levels out.

It is important to note that the tail turning is limited by the torque of the motor. If the motor torque increased, higher turning rates would be achieved. Additionally, if the robot is able to run with an airborne phase, the effective coefficient of friction could be zero during tail actuation on any terrain. Also, the legged results are theoretical, and the best published yaw rates of $230°s^{-1}$have been shown using legs in [20].

IV. Experimental Results

A. Robot in Free Fall

To test the maximum possible performance of the tail, the tail was actuated at maximum effort for 150 milliseconds while the robot was in free fall. This provides a zero angular momentum environment in which the robot can turn, serving as a benchmark for terrestrial turning as well as a check on the model. In Figure 9 we see the results of this experiment and a comparison to the model discussed in Section III.

The model accurately matches the results of the experiment. In the experiment, the robot turns at an average of $447°s^{-1}$, compared to $530°s^{-1}$for the model. Much of the difference may be due to the fact that the motor does not start developing torque exactly at zero seconds in the experiment. If we assume a lag of 5 milliseconds, there is almost no discrepancy. The turning rate of $530°s^{-1}$represents an upper bound on performance with respect to our model, although unmodeled effects while the robot is on the ground, such as leg compliance, could increase the turning rate beyond this limit.

B. Effect of Running Speed on Tail Efficacy with Open Loop Actuation

For agile locomotion, it may be desirable to run the robot at a range of speeds. Experiments were performed to determine how the performance of the tail system varied with running frequency. If the variance were low, open loop control with the tail could be possible. Additionally, these tests would reveal the maximum change in body angle that could be produced by the tail at various leg frequencies. Experiments consisted of the robot running straight for one second with leg steering control [24] activated, then simultaneously turning off the leg steering control and actuating the tail at maximum effort. The tail actuation induces a turn in the robot, which is measured with the MEMS gyroscope. The experiment was done over irregular floor tile, at 8 different leg frequencies between 0 and 13.3 Hz. At each leg frequency considered, 10 trials were performed for a total of 80 experiments. Leg frequencies between 0 and 3 Hz are not well controlled and were not tested.

Figure 10 shows the results of these experiments. As leg frequency increases, the effective coefficient of friction generally decreases and then levels off at high frequencies, as shown in [24]. This produces a higher body yaw rate at higher leg frequencies, from $296°s^{-1}$at standstill to $344°s^{-1}$at 3.3 Hz to $401°s^{-1}$at 10 Hz. A possible explanation for the decrease and leveling off of the coefficient of friction is that at low frequencies, the legs are sticking and slipping, yielding a coefficient of friction somewhere between that of static and dynamic. At higher frequencies slip dominates and only dynamic friction is observed. A Student's t-test reveals statistically significant differences ($p<.05$) between 3.3 Hz, 6.7 Hz, and 8.3 Hz, while the turning rates at higher frequencies are not statistically significantly different from each other.

As shown in Figure 10, the model matches the experiments well for trials where the robot is running forward. At 10 Hz leg frequency, the error is 1.5%. At 5 Hz the model performs the worst, with an error of 13.4%. The total average error is 3.5%. For trials at 0 Hz, the model does not match the experiment well, with an error of -50%. The robot body is able to shift without the legs moving, as the hip flexures act as springs. This may explain the discrepancy, and a more appropriate model may be a rigid body rotating on a torsional spring.

It is also interesting to note places where the experiment slightly outperforms the model - most models are idealizations and show better than real-world performance. For this work the stochastic nature of the leg contact means that the friction used in the model could be overestimated. For example, if the robot's airborne phase is significant during the tail flick, this may lead to lower overall friction, since the full weight of the robot and tail is not on the legs at all times. This variation shows that consistent turning cannot be done open loop, and feedback control is necessary.

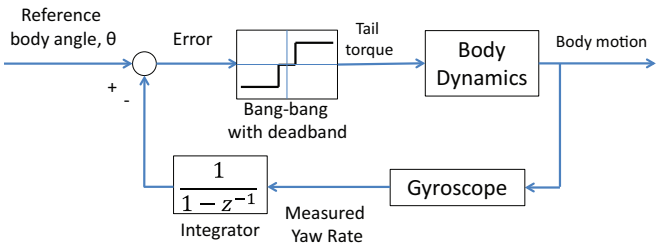

Fig. 11. Control block diagram for the body angle control. The tail is given maximum positive or negative torque when away from the reference angle, and given zero torque in a small deadband to prevent unwanted high frequency actuation.

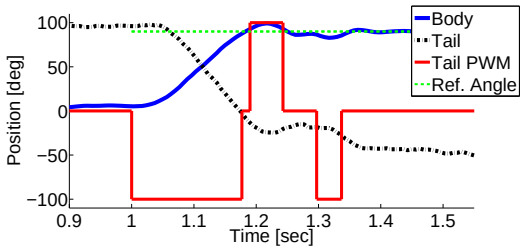

Fig. 12. The tail motion induces a turn in the body. The bang-bang controller reacts to any overshoot by reversing the direction of the tail movement. A controlled 90 degree turn is performed in about 0.25 seconds. Body position measured using onboard MEMS gyroscope, tail position measured using absolute position encoder.

V. Tail and Body Control

A. Relative Position Control of the Tail

The Hall effect sensor on the tail allows us to execute a standard PID control loop on the position of the tail relative to the body. The controller can execute quick and accurate tail commands. For a 90 degree step change in commanded position, the tail has a 5% settling time of 0.46 seconds and a steady state error of 2.2 degrees.

Due to the limited range of motion of the tail, this functionality is important if the tail is to execute a large maneuver. For example, if the robot is to be turned 90 degrees using only the tail, the tail should start near the end of its range of motion, or it may collide with the stop before the 90 degree goal can be reached.

B. Body Angle Control using the Tail and Gyroscope Feedback

We implemented a control mode on the tail where it will produce a turn of the body rapidly using feedback from the gyroscope. The body can be turned up to 90 degrees using this method, before the tail saturates. After tail saturation, the legs would have to be engaged to turn the robot further, or the tail would have to be reset so it can be actuated again.

Due to the varying friction, it is difficult to establish an input/output map of tail motion to body motion. Thus, a PID controller would be difficult to implement. Instead, we use a "bang-bang" controller, shown in Figure 11, applying maximum torque to the tail unless the body is within five degrees of the goal angle. This serves as a deadband, and no torque is applied. The deadband also ensures that the tail is not actuated due to small oscillations in the gyroscope. Furthermore, the body position feedback is a forward Euler integration of the gyroscope readings, which serves as a filter that eliminates almost all of the measurement noise. This method of measuring position was verified using an OptiTrack motion capture system [2], and it is as accurate as said system. Using maximum torque ensures that the static friction is overcome and that the robot operates in the dynamic friction regime. This allows the robot to make turns of up to 90 degrees without the tail saturating, depending on the robot's forward speed. Using this gyro based control, the robot can make a controlled 90 degree turn in one quarter of a second, as shown in Figure 12.

The bang-bang controller is able to remove much of the variation seen in open loop actuation. 10 trials each of 30, 60, and 90° commands were performed as the robot was running forward with a 10 Hz leg frequency. Forward speed was not controlled (only leg frequency) but for most trials the speed was approximately 32 $cmsec^{-1}$. While running forward, the robot keeps a straight heading using legged steering control as presented in [24]. As shown in Table I, for 30 and 60° turns the RMS error (calculated using the error at the end of the 0.33 s period for which the controller is turned on) is less than five degrees, the size of the control deadband. Control becomes difficult at more extreme angles. At 90° the RMS error is over 13°. With high friction, the tail rotates more quickly relative to the body, meaning that the tail's range of motion may be consumed before reaching the target angle. If this occurs, the tail collides with the housing, creating an impulsive moment, turning the robot away from the target angle. This leads to large errors, but an increased range of motion could eliminate this problem. This occurred in a single trial, denoted by the black cross on Figure 13.

TABLE I
RMS error and commanded angle.

Commanded Angle	RMS Error
30°	3.8°
60°	4.5°
90°	13.2°

C. Comparison of Tail Control to Leg Differential Drive Control

This method of controlling the body angle with tail actuation is precise and rapid, and makes sharper turns in shorter time compared with other methods. Figure 14 shows the path the robot takes while executing a 90 degree turn. Paths were measured using the OptiTrack motion capture system. Three methods are used to make the turn, all executed while the robot moves forward with a 10 Hz leg frequency, with a forward velocity of approximately 30 $cmsec^{-1}$. The first method employs differential drive (legged) steering with

[2]http://www.naturalpoint.com/optitrack/

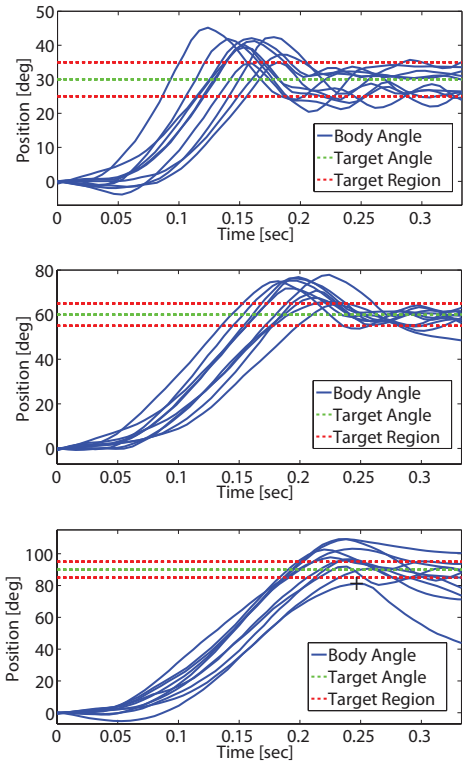

Fig. 13. Results of the bang-bang controller commanded to 30, 60, and 90° turns. 10 trials for each target angle. The black cross shows where, in one trial, the tail reached the end of its range of motion, creating an internal impact and turning the robot away from the target angle.

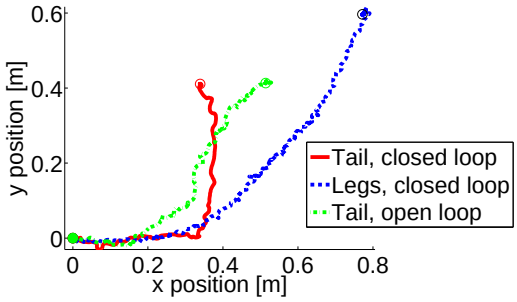

Fig. 14. Path of the robot as it runs forward, executes a 90 degree turn, and runs forward again. Turns performed on tile surface.

gyroscope feedback. Using leg kinematics we can accurately turn the robot 90 degrees, but the path required is much larger and the time required is three times greater than using the tail. The second method used is by actuating the tail without feedback. This results in a quick, sharp, but inaccurate turn. Finally, the robot is turned using the tail with gyroscope feedback. Using this method, we achieve a 90 degree turn in 1/3 of a second with a turning radius of 4 cm. Figure 15 shows the robot position, heading, and speed while the closed loop tail control is actuated. The origin of the arrow is the robot position, the direction of the arrow is the robot's heading, and the length of the arrow is proportional to the robot's velocity.

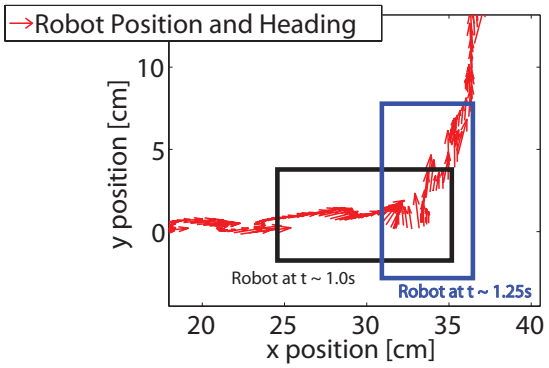

Fig. 15. A zoomed-in look at Figure 14, displaying data from the closed loop tail trial. The origin of the arrow is the robot position, the direction of the arrow is the robot's heading, and the length of the arrow is proportional to the robot's velocity. The robot makes a 90 degree turn in the space of approximately 4 cm, or 0.4 body lengths, without slowing down.

VI. Discussion and Conclusions

TAYLRoACH is able to make 90° turns from straight line motion in 0.25 seconds with precision in less than half of a body length, while running forward at over 3 body lengths per second. For uncontrolled turns, the robot can turn at $400°s^{-1}$. To the author's knowledge, no other legged robot can match this turning performance. Table II shows the size and yaw rates of some other legged robots.

TABLE II

A yaw rate comparison among dynamic legged robots.

Robot	Size cm	Mass (gm)	Yaw Rate ($°s^{-1}$)	Speed ms^{-1}
miniRoACH [6]	3	2.4	86	0.03
DASH [2]	10	20	50	1.5
dynaRoACH [7]	10	30	100	1.4
iSprawl [12]	16	300	230	2.3
OctoRoACH [24]	13	36	90	0.5
RHex [25]	53	7000	40	2.7
TAYLRoACH	10	46	400	1.0

TAYLRoACH achieves this high performance using its tail to produce large changes in angular momentum in a short time. While previous work has shown that it is possible to produce turns using this method, controlled turns of this radius have not been previously shown. Additionally, the robot can make these turns while the running at high speeds without significantly slowing down. Other methods have difficulty turning while the robot runs forward and show decreased performance as running speed increases. An example of a controlled, rapid turn can be seen in figure 16.

Variable friction forces encountered by the robot make closed loop control necessary for precision turns. The bang-bang controller presented here is a simple and effective solution when stiction is involved. Due to its excellent turning capabilities, TAYLRoACH has the potential to quickly navigate through small spaces where other robots could not. In a search and rescue situation, where a robot may face many small constrictions, and time is of the essence, the ability to make quick, accurate turns on slippery surfaces

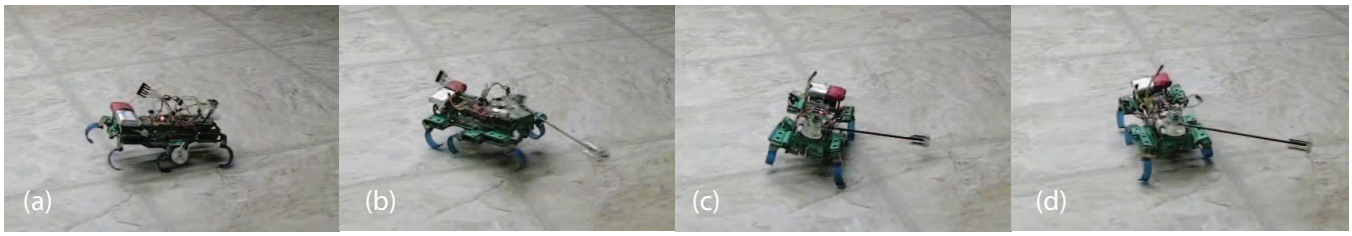

Fig. 16. TAYLRoACH makes a controlled 90 degree turn on a tile surface. (a) Tail starts to move [t = 0.0s] (b) Robot about halfway through turn [t = 0.14s] (c) Robot overshoots 90° target [t = 0.23s] (d) Tail corrects overshoot, robot has made 90° turn [t = 0.30s]

while running could be critical.

Turning with a tail is rich subject, and not all elements of it are addressed here. After a single turn, the range of motion of the tail is often consumed, making two consecutive turns in the same direction not possible. This could be solved by either a slow "reset tail position" command (due to static friction, moving the tail slowly will not move the body) or by developing a tail with an unlimited range of motion. Additionally, the interaction of the leg contact forces and the tail actuation could be examined, possibly allowing greater turning ability with proper timing. Additionally, the interaction of the leg contact forces and the tail actuation should be examined, possibly allowing greater turning ability with proper timing. Analysis of combined leg and tail turning is likely terrain dependent, but should lead to effective control strategies for highly dynamic maneuvering.

VII. Acknowledgements

Thanks to K. Peterson, A. Gillies, and F. Garcia Bermudez for obtaining the motor testing data, inspiring Figure 15, and video editing help, respectively.

References

[1] S. Bergbreiter, "Autonomous jumping microrobots," Ph.D. dissertation, University of California, Berkeley, 2007.

[2] P. Birkmeyer, K. Peterson, and R. S. Fearing, "DASH: A dynamic 16g hexapedal robot," in *IEEE Int. Conf. on Intelligent Robots and Systems*, St. Louis, MO, 2009.

[3] J. G. Cham, S. A. Bailey, J. E. Clark, R. J. Full, and M. R. Cutkosky, "Fast and robust: Hexapedal robots via shape deposition manufacturing," *The Int. Journal of Robotics Research*, vol. 21, no. 10-11, pp. 869–882, 2002.

[4] E. Chang-Siu, T. Libby, M. Tomizuka, and R. Full, "A lizard-inspired active tail enables rapid maneuvers and dynamic stabilization in a terrestrial robot," in *IEEE Int. Conf. on Intelligent Robots and Systems*, September 2011.

[5] K. Hirata, T. Takimoto, and K. Tamura, "Study on turning performance of a fish robot," *First International Symposium on Aqua Bio-Mechanisms*, 2002.

[6] A. M. Hoover, E. Steltz, and R. S. Fearing, "Roach: An autonomous 2.4g crawling hexapod robot," in *IEEE Int. Conf. on Intelligent Robots and Systems*, Nice, France, Sept. 2008.

[7] A. Hoover, S. Burden, X.-Y. Fu, S. Sastry, and R. Fearing, "Bio-inspired design and dynamic maneuverability of a minimally actuated six-legged robot," in *IEEE Int. Conf. on Biomedical Robotics and Biomechatronics.*, Sep. 2010.

[8] A. Hoover and R. Fearing, "Analysis of off-axis performance of compliant mechanisms with applications to mobile millirobot design," in *IEEE/RSJ Int. Conf. on Intelligent Robots and Systems, 2009.*, Oct. 2009, pp. 2770 –2776.

[9] A. Johnson, T. Libby, E. Chang-Siu, M. Tomizuka, R. Full, and D. Koditschek, "Tail assisted dynamic self righting," in *15th Int. Conf. on Climbing and Walking Robots (CLAWAR)*, July 2012.

[10] A. Jusufi, D. T. Kawano, T. Libby, and R. J. Full, "Righting and turning in mid-air using appendage inertia: reptile tails, analytical models and bio-inspired robots," *Bioinspiration & Biomimetics*, vol. 5, no. 4, p. 045001, 2010.

[11] S. Kim, A. T. Asbeck, M. R. Cutkosky, and W. R. Provancher, "SpinybotII: Climbing hard walls with compliant microspines," in *12th Intl Conf on Advanced Robotics*, 2005, pp. 601–606.

[12] S. Kim, J. E. Clark, and M. R. Cutkosky, "iSprawl: Design and tuning for high-speed autonomous open-loop running," *The Int. Journal of Robotics Research*, vol. 25, no. 9, pp. 903–912, 2006.

[13] J.-S. Koh and K.-J. Cho, "Omegabot : Biomimetic inchworm robot using sma coil actuator and smart composite microstructures (SCM)," in *IEEE Int. Conf. on Robotics and Biomimetics*, Dec. 2009, pp. 1154 –1159.

[14] N. Kohut, D. Haldane, D. Zarrouk, and R. Fearing, in *15th Int. Conf. on Climbing and Walking Robots (CLAWAR)*.

[15] N. Kohut, A. Hoover, K. Ma, S. Baek, and R. Fearing, "Medic: A legged millirobot utilizing novel obstacle traversal," in *IEEE Int. Conf. on Robotics and Automation*, May 2011.

[16] M. Kovač, M. Schlegel, J.-C. Zufferey, and D. Floreano, "Steerable miniature jumping robot," *Autonomous Robots*, vol. 28, no. 3, pp. 295–306, 2010.

[17] D. Lee, S. Kim, Y.-L. Park, and R. Wood, "Design of centimeter-scale inchworm robots with bidirectional claws," in *IEEE Int. Conf. on Robotics and Automation*, May 2011, pp. 3197 –3204.

[18] T. Libby, T. Moore, E. Chang-Siu, D. Li, D. Cohen, A. Jusufi, and R. Full, "Tail-assisted pitch control in lizards, robots and dinosaurs," *Nature*, vol. 481, pp. 181–184, 2012.

[19] G. A. Lynch, J. Clark, P. Lin, and D. Koditschek, "A bioinspired dynamical vertical climbing robot," *Int. Journal of Robotics Research*, vol. 31, pp. 974–976, 2012.

[20] A. McClung, "Techniques for dynamic maneuvering of hexapedal legged robots," Ph.D. dissertation, Stanford University, 2006.

[21] C. Ordonez, N. Gupta, E. Collins Jr., and J. Clark, "Power modeling of the XRL hexapedal robot and its application to energy efficient motion planning," in *15th Int. Conf. on Climbing and Walking Robots (CLAWAR)*, July 2012.

[22] K. Peterson and R. S. Fearing, "Experimental dynamics of wing assisted running for a bipedal ornithopter," in *IEEE Int. Conf. on Intelligent Robots and Systems*, Sept. 2011, pp. 5080 –5086.

[23] W. Provancher, S. Jensen-Segal, and M. Fehlberg, "Rocr: An energy-efficient dynamic wall-climbing robot," *Mechatronics, IEEE/ASME Transactions on*, vol. 16, no. 5, pp. 897 –906, Oct. 2011.

[24] A. Pullin, N. Kohut, D. Zarrouk, and R. Fearing, "Dynamic turning of 13 cm robot comparing tail and differential drive," in *IEEE Int. Conf. on Robotics and Automation*, May 2012.

[25] U. Saranli, M. Buehler, and D. E. Koditschek, "RHex: A simple and highly mobile hexapod robot," *The Int. J. of Robotics Research*, vol. 20, no. 7, pp. 616–631, 2001.

[26] M. Spenko, G. Haynes, J. Saunders, M. Cutkosky, A. Rizzi, R. Full, and D. Koditschek, "Biologically inspired climbing with a hexapedal robot," *Journal of Field Robotics*, vol. 25, pp. 223 –242, 2008.

[27] K. Yamafuji, T. Kawmura, and M. Feng, "Elucidation of twisting motion of a falling cat and realization of cat-turn motion by a robot," in *International Symposium on Robotics*, vol. 30, October 2004.